

Model-based Q Factor Control for Photothermally Excited Microcantilevers

Michael G. Ruppert¹, Ben S. Routley¹, Andrew J. Fleming¹, Yuen K. Yong¹, and Georg E. Fantner²

Abstract—Photothermal excitation of the cantilever for dynamic atomic force microscopy (AFM) modes is an attractive actuation method as it provides clean cantilever actuation leading to well-defined frequency responses. Unlike conventional piezo-acoustic excitation of the cantilever, it allows for model-based quality (Q) factor control in order to increase the cantilever tracking bandwidth for tapping-mode AFM or to reduce resonant ringing for high-speed photothermal off-resonance tapping (PORT) in ambient conditions. In this work, we present system identification, controller design and experimental results on controlling the Q factor of a photothermally driven cantilever. The work is expected to lay the groundwork for future implementations for high-speed PORT imaging in ambient conditions.

Index Terms—Atomic Force Microscopy, Photothermal Actuation, Vibration Control, System Identification, Controller Design

I. INTRODUCTION

Atomic force microscopy (AFM) [1] has significantly enabled the steady growth of nanotechnology over the past three decades. As a key instrument for visualizing the nano-scale properties of a variety of samples, the AFM has produced images of strings of DNA, cells, proteins and polymers [2] and demonstrated true atomic resolution [3]. At the core of the instrument, a microcantilever forms the physical link between the sample under investigation and the measurable quantity. By scanning the cantilever with a sharp tip over the surface of the sample and maintaining a constant setpoint with a feedback controller, a three dimensional image of the sample's topography is obtained.

A number of operating modes have been demonstrated over the years, which, depending on the type of cantilever actuation, can be broadly classified in static (contact-mode) and dynamic (resonance and off-resonance) techniques. The earliest and most common form of operation is contact-mode AFM (CM-AFM) [1] which can be employed for fast measurements of hard samples, however it will damage soft and biological samples and lead to wear and tear of the probe tip [4]. This disadvantage arising from lateral friction forces was overcome by operating the AFM in dynamic modes through the excitation at or near the cantilever's fundamental flexural

resonance frequency. For operation in ambient conditions and liquid environments, tapping-mode AFM [5], for which the controller maintains a constant cantilever amplitude, has established itself as the standard operating mode for investigating biologically-relevant samples [6].

However, tapping-mode AFM in air is inherently slow, pre-dominantly limited by the slow amplitude dynamics of cantilever resulting from the high quality (Q) factor. As such, high-speed experiments in order to study dynamic biological processes with molecular resolution have only been obtained in liquid environments [7]–[9] where the Q factor naturally drops to very small values. Moreover, it was recently shown that for very weakly bound biological molecules, high-speed tapping-mode AFM does not provide gentle enough imaging conditions to visualize the highly delicate assembly processes [10]. Instead, AFM based on cycle-to-cycle feedback directly from the tip-sample force [11] can provide the necessary low force set points in order to observe these processes [10], [12], [13].

In order to make full use of the potential of this imaging mode, high-speed actuation of the cantilever away from the resonance is required. In conventional approaches, this is achieved by the z-stage driven by a piezoelectric stack actuator which in turn usually has a relatively low bandwidth [14]. In contrast, photothermal actuation of the cantilever [15] has the potential to achieve several hundreds of kilohertz of bandwidth in the vertical direction and is only limited by the cantilever resonance frequency. In liquid environments, this is hardly a problem as the resonance is heavily damped by the surrounding medium. However, in ambient conditions, the vertical bandwidth is limited by the high Q factor of the cantilever which causes a significant transient response and ringing after contact with the sample.

II. Q CONTROL OF MICROCANTILEVERS

Q control was originally introduced to modify the quality factor of the fundamental mode of the cantilever [16], which lead to a number of advances in tapping-mode AFM. By actively damping the cantilever resonance, an increase in scan speed is achieved [17]–[19] as a result of increasing the cantilever tracking bandwidth which allows for larger z-axis feedback controller gains.

A. Time-Delay Q Control

Active modification of the cantilever Q factor is realized by velocity feedback. As most commercial AFM systems only provide a position sensor to measure the cantilever deflection, velocity at the resonance frequency has to be

*This work was supported by the Australian Research Council and the European Union H2020 Framework Programme for Research & Innovation (2014-2020), ERC-2017-CoG, InCell, Project number 773091 (to G.E.F.).

¹M. G. Ruppert, B. S. Routley, A. J. Fleming, and Y. K. Yong are with the School of Electrical Engineering and Computing, The University of Newcastle, Callaghan, Australia michael.ruppert@newcastle.edu.au

²G. E. Fantner is with the Laboratory for Bio- and Nano-Instrumentation, École polytechnique fédérale de Lausanne, Lausanne, Switzerland georg.fantner@epfl.ch

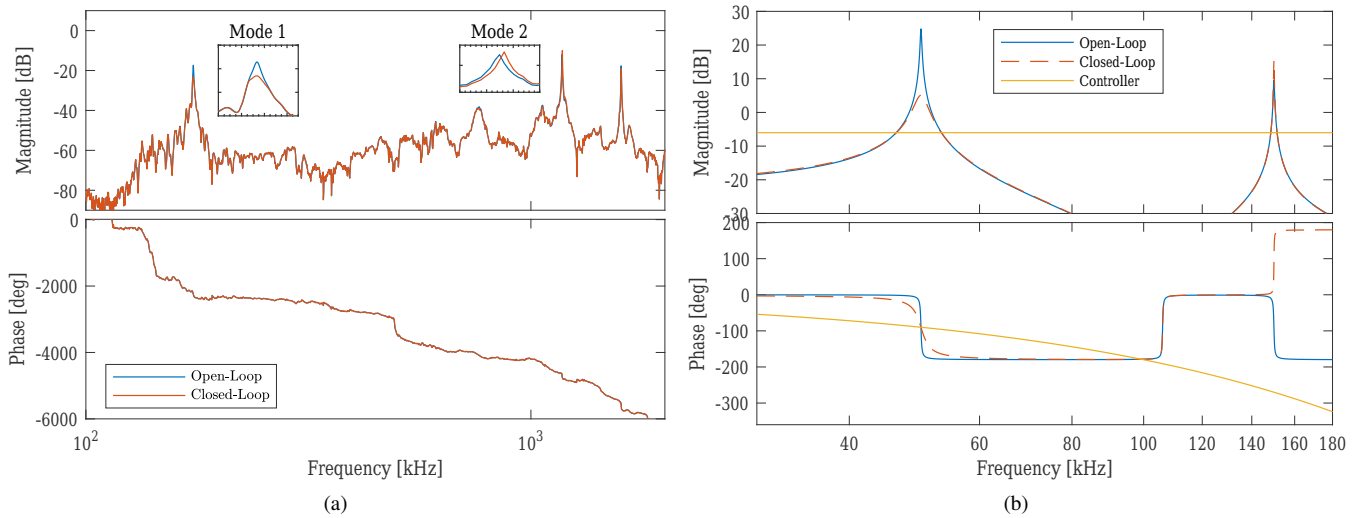


Fig. 1. (a) Experimentally obtained frequency response of a piezo-acoustically actuated cantilever with time-delay feedback controller for Q reduction on the first mode. (b) Simulated frequency response of a multimode cantilever with time-delay feedback control showing instability on the second eigenmode due to spillover.

approximated from the displacement signal. Since the displacement signal is sinusoidal, a velocity estimate is obtained by applying a phase-shift of -90° and a corresponding gain to the displacement signal. This approach is most commonly realized through a time-delay controller of the form [20]

$$K(s) = ge^{-T_d s} \quad (1)$$

where g is the gain and $T_d = \frac{90^\circ}{360^\circ} \frac{1}{f_0}$ is the time-delay as a function of the resonance frequency. This approach remains an easy to implement solution for practitioners and is by far the most widely used Q control approach reported in literature. However, the time-delay approach is severely limited as it comes with a number of disadvantages such as the restriction to controlling a single mode [19], and non-robust stability properties [21] leading to spill-over at higher order eigenmodes [22]–[24].

In practice, most commercial AFM systems will utilize a piezo-acoustic excitation at the base of the cantilever leading to a frequency response as is shown in Fig. 1(a). The numerous additional complex dynamics and higher order modes from the mechanical mounting will inherently limit the achievable controller performance of the time-delay method. In this example, an initial Q factor of the first mode of $Q = 281$ can only be reduced to $Q^* = 124$ with a gain of $g = -7$ before spill-over renders the cantilever system unstable at the higher eigenmode. This phenomenon is observable at the increased second mode Q factor due to the control action on the first mode. Since the frequency response of the time-delay controller exhibits a continuously dropping phase, it may happen that at a higher (unmodeled) eigenmode the phase is a πn multiple of -90° . This in turn is equivalent to a negative gain which leads to positive feedback and in the worst case destabilizes the system as demonstrated in Fig. 1(b).

B. Model-based Q Control

This problem can be overcome by using integrated actuation, for instance via a piezoelectric layer which enables the utilization of resonant controllers [24]. This approach allows for the control of multiple eigenmodes in parallel in order to enable imaging on higher eigenmodes [19] or to influence the material contrast in bimodal AFM [25]. If additionally, the optical beam deflection sensor is replaced by an integrated sensor such as piezoelectric sensing [26]–[29], a collocated system is obtained [30] and vibration control for reducing the Q factor results in guaranteed robust stability properties of the closed loop [31].

C. Contribution

Enabled by the clean actuation of the photothermal excitation, we demonstrate model-based Q control in this work to alleviate the problem of resonant ringing of the cantilever after sample contact for high-speed photothermal off-resonance tapping (PORT) [10]. In this approach, a Q controller is designed to dampen the first eigenmode of the cantilever without affecting the response of the cantilever off resonance and at lower frequencies. The controller is designed to be of low order to be suitable for implementation on a field programmable analog array (FPAA).

III. PHOTOTHERMAL Q CONTROL

A. Experimental Setup

The experimental setup consists of a modified Horiba XploRA Nano Raman spectrometer with an AJST-NT scanning probe microscope. In order to enable photothermal excitation, the Raman laser diode with a wavelength of 638 nm and an output power of 22 mW was used as the excitation laser. The output from this laser was amplitude modulated via an acoustic optical modulator (AOM). A 10x objective lens was used to focus the modulated laser beam to a diffraction limited spot ($1 \mu\text{m}$) at the base of

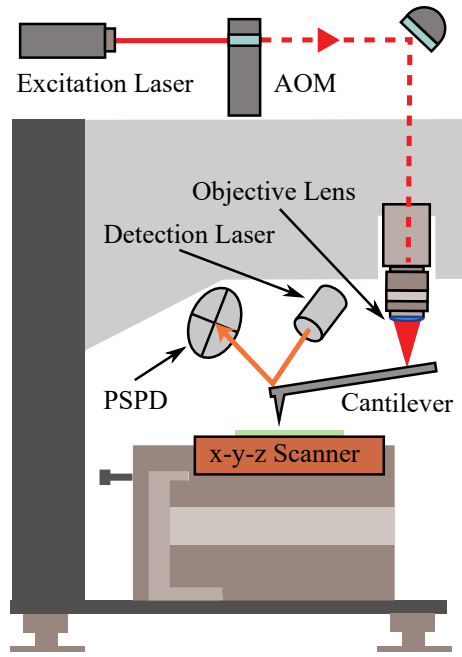


Fig. 2. Schematic setup of the photothermal excitation system.

the cantilever. As the detection laser has a wavelength of 1000 nm and the position sensitive photo detector (PSPD) has an optical bandpass filter, interferences between the excitation and detection systems are avoided. An overview of the detection and excitation systems is shown in Fig. 2.

B. System Identification

The cantilevers investigated in this work are general purpose tapping-mode cantilevers (Micromasch, HQ:NSC). Frequency responses are obtained by performing a sinusoidal frequency sweep of the amplitude modulation of the AOM with a DC offset of 2.5 V (signal range 0V – 5V) and measuring the response with a optical beam deflection sensor demodulated using a lock-in amplifier (Zurich Instruments, HF2LI). Examples of three different cantilevers are shown in Fig. 3.

A common property of the photothermal actuation is a low-pass roll-off because both, the temperature at the illuminated position, and the thermal diffusion length decrease as the modulation frequency increases [32]. These dynamics need to be taken into account for controller design. System identification is performed from frequency domain data. The measured frequency response data (FRD) along with a third order (model 1) and fourth order model (model 2) are shown in Fig. 4. Here, model 1 is chosen as a series connection of a low-pass filter and a second order resonant transfer function and is of the form

$$H(s) = F(s)G(s) = \frac{s + z_1}{s + p_1} \frac{\alpha \omega_0^2}{s^2 + \frac{\omega_0}{Q}s + \omega_0^2} \quad (2)$$

where α, ω_0, Q are the gain, resonance frequency and quality factor of the resonance and z_i, p_i are the zeros and poles of the filter $F(s)$. From the model, the resonance

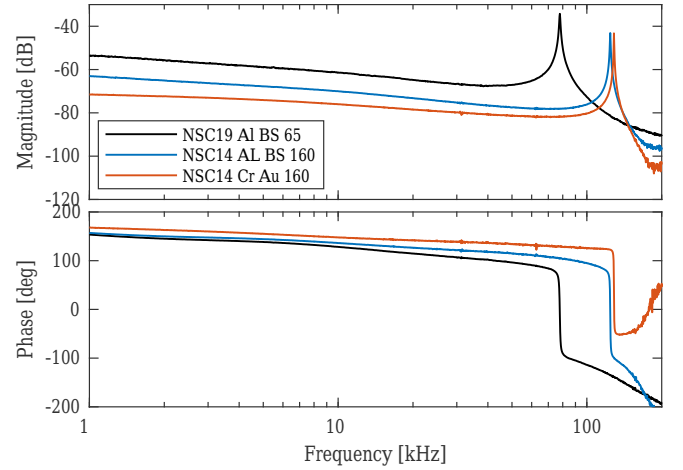


Fig. 3. Measured frequency responses of three photothermally excited cantilevers.

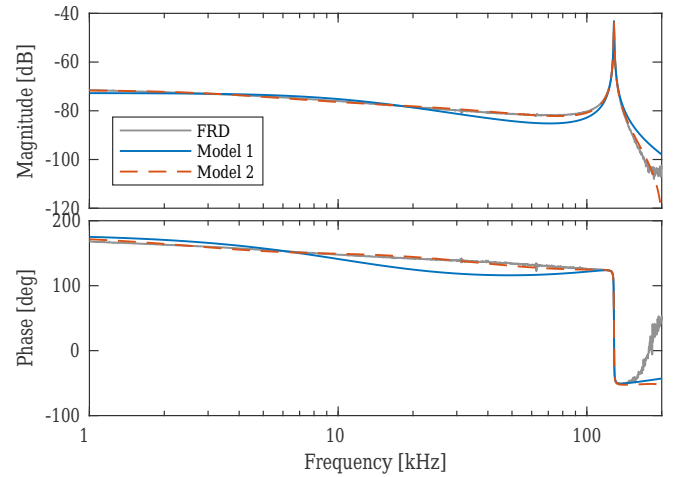


Fig. 4. Measured frequency response of the photothermally excited cantilever (NSC14 Cr Au 160) (black), first-order lowpass filter model with one zero (blue) (2) and full fourth-order transfer function model (red).

frequency $f_0 = 128.5$ kHz and quality factor $Q = 290$ are found for the NSC14 Cr Au 160 cantilever which is considered in the remainder of this work. While a better fit is obtained with a full fourth-order transfer function (Model 2), it would yield to a higher order Q controller and is therefore not considered in the following sections.

C. Controller Design: Observer-based Approach

The purpose of the Q controller is to add damping to the resonance of the cantilever. This is achieved by increasing the negative real part of the complex conjugate pole pair associated with the first eigenmode while leaving the resonance frequency unchanged. The poles of the open-loop system sorted in ascending order are given by $p = [p_1, p_2, p_3]$ where

$$p_{2,3} = \frac{-\omega_0}{2Q} \pm j\omega_0 \sqrt{1 - \frac{1}{4Q^2}}. \quad (3)$$

In order to add damping to the resonance, only the complex conjugate pole-pair of the resonance $p_{2,3}$ are shifted deeper into the left half plane. The desired closed-loop poles are

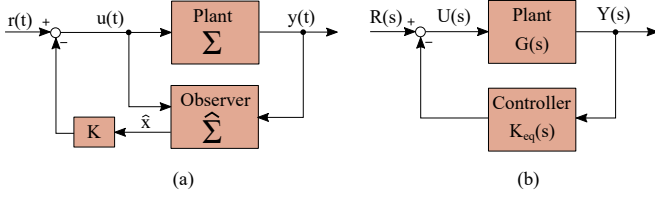


Fig. 5. Block diagram of (a) observer based stated feedback and (b) equivalent feedback controller architecture.

calculated as $p = [p_1, r_d + \Im\{p_2\}, r_d + \Im\{p_3\}]$ where $r_d = -\omega_0/(2Q_d)$ and Q_d is the desired Q factor.

If the system (2) is written in state-space form

$$\Sigma: \begin{aligned} \dot{x} &= Ax + Bu \\ y &= Cx + Du \end{aligned} \quad (4)$$

and the pair (A, B) is controllable, then there exists a feedback matrix K such that $u = -Kx + r$ assigns arbitrary closed-loop poles to the system (4) [33]. However, proportional feedback of the states requires that all states are available for measurement and this is usually not the case. Therefore, feedback from the estimated states using a Luenberger observer as shown in the block diagram in Fig. 5(a) can be employed. The resulting system is a two-input / one-output controller with inputs $[u \quad y]$ of the form

$$\hat{\Sigma}: \begin{aligned} \dot{\hat{x}} &= (A - LC)\hat{x} + [B - LD \quad L] \begin{bmatrix} u \\ y \end{bmatrix} \\ u &= -K\hat{x} + r. \end{aligned} \quad (5)$$

Here K is chosen in the same manner as for full state feedback and L is chosen such that the observer poles are 2 – 5 times faster than the closed-loop poles [34]. This is to ensure that the estimation error converges to zero faster than the plant dynamics without introducing excessive measurement noise into the estimated states. Taking the Laplace transform of (5) yields the equivalent single-input / single-output controller

$$K_{eq}(s) = \frac{U(s)}{Y(s)} = -K(sI - (A - LC - BK))^{-1}L. \quad (6)$$

The resulting block diagram is shown in Fig. 5(b). A simulation of the closed loop with the equivalent controller resulting from observer-based state feedback is shown in Fig. 6. Here, the first order low-pass filter model for the cantilever shown in Fig. 4 is used and the desired Q factor is $Q_d = 10$. The resulting equivalent controller is simulated with the model and the actual frequency response data (FRD). In both cases, the Q factor is reduced from $Q = 290$ to $Q^* = 9$. From Fig. 6(b), it can be seen that the equivalent controller has a complex-conjugate pole-pair at high frequencies corresponding to observer dynamics originating from the controller design.

D. Controller Design: Pole-placement Approach

The controller design using the observer-based approach yields a third order controller with high-frequency dynamics

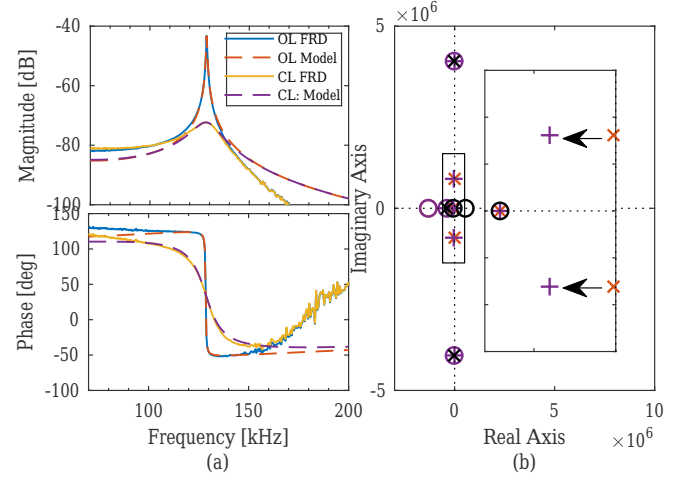


Fig. 6. (a) Bode plot and (b) pole-zero map of open and closed loop using observer-based state feedback and using the equivalent controller from (6). The poles and zeros of (6) are also shown in (b) in black.

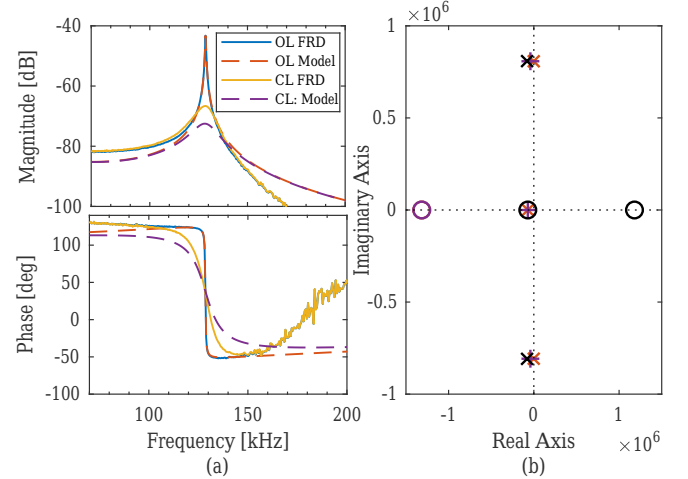


Fig. 7. (a) Bode plot and (b) pole-zero map of open and closed loop using direct polynomial pole placement. The poles and zeros of (10) are also shown in (b) in black.

which are not possible to be implemented with a field programmable analog array (FPAA). However, pole placement can be directly performed by working directly with the estimated transfer function polynomials. In this approach, a model and controller of the form

$$\begin{aligned} H_0(s) &= \frac{B_0(s)}{A_0(s)} = \frac{b_n s^n + \dots + b_0}{a_n s^n + \dots + a_0} \\ C(s) &= \frac{P(s)}{L(s)} = \frac{p_{n-1} s^{n-1} + \dots + p_0}{l_{n-1} s^{n-1} + \dots + l_0} \end{aligned} \quad (7)$$

are considered. If the denominator degree is given by $n = \deg(A_0(s))$, then a controller with polynomial degrees $n_p = \deg(P(s)) = n - 1$ and $n_l = \deg(L(s)) = n - 1$ allows for an arbitrary choice of a closed-loop polynomial of the form [33]

$$A_{cl}(s) = L(s)A_0(s) + P(s)B_0(s) \quad (8)$$

where the degree of the closed-loop denominator polynomial

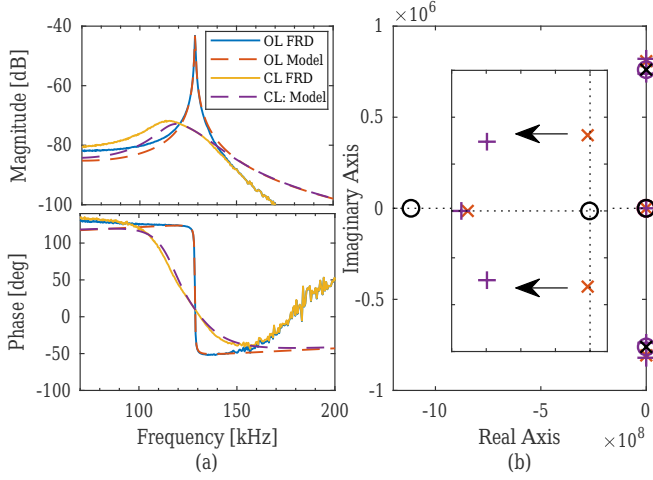


Fig. 8. (a) Bode plot and (b) pole-zero map of open and closed loop using H_∞ -norm minimization. The poles and zeros of (10) are also shown in (b) in black.

is $n_c = 2n - 1$. The controller polynomials are found by solving the following equation

$$\begin{bmatrix} a_n & 0 & \dots & 0 & b_n & 0 & \dots & 0 \\ a_{n-1} & a_n & \dots & 0 & b_{n-1} & b_n & \dots & 0 \\ \vdots & \vdots & \ddots & \vdots & \vdots & \vdots & \ddots & \vdots \\ a_0 & a_1 & \dots & a_n & b_0 & b_1 & \dots & b_n \\ 0 & a_0 & \dots & a_{n-1} & 0 & b_0 & \dots & b_{n-1} \\ \vdots & \vdots & \ddots & \vdots & \vdots & \vdots & \ddots & \vdots \\ 0 & 0 & \dots & a_0 & 0 & 0 & \dots & b_0 \end{bmatrix} \begin{bmatrix} l_{n-1} \\ \vdots \\ l_0 \\ p_{n-1} \\ \vdots \\ p_0 \end{bmatrix} = \begin{bmatrix} a_{n_c}^c \\ \vdots \\ a_0^c \end{bmatrix} \quad (9)$$

where a_i^c are the coefficient of the closed-loop polynomial (8). For the given system, the degrees of the polynomials calculate to $n = 3, n_p = n_l = 2, n_c = 5$ and hence the controller has the following form

$$C(s) = \frac{P(s)}{L(s)} = \frac{p_2 s^2 + p_1 s + p_0}{l_2 s^2 + l_1 s + l_0}. \quad (10)$$

The desired polynomial is chosen in a similar fashion as discussed in Section III-C by leaving the real pole unaltered and placing the complex-conjugate pole pair deeper into the left half plane.

The simulation results with the model and the FRD data is shown in Fig. 7. The resulting Q factor of the closed-loop FRD model is $Q^* = 13.8$. This approach avoids the high-frequency controller dynamics and yields a minimal controller realization. However, calculation the matrix inverse of (9) can be badly conditioned for highly resonant systems like the cantilever.

E. Controller Design: H_∞ -Norm Optimization

Given a prototype controller of the form (10), controller design to find the maximum damping Q controller can also be stated as an optimization problem of the form

$$\min_{p_i, z_i} \|G_{cl}(j\omega)\|_\infty \quad (11)$$

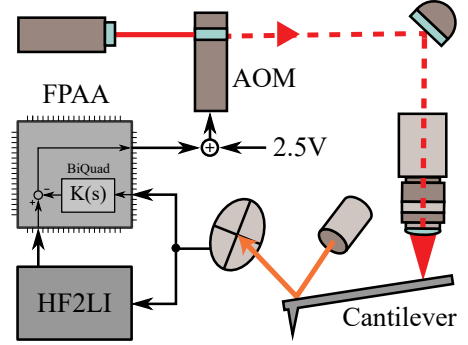


Fig. 9. Schematic experimental setup for photothermal Q control.

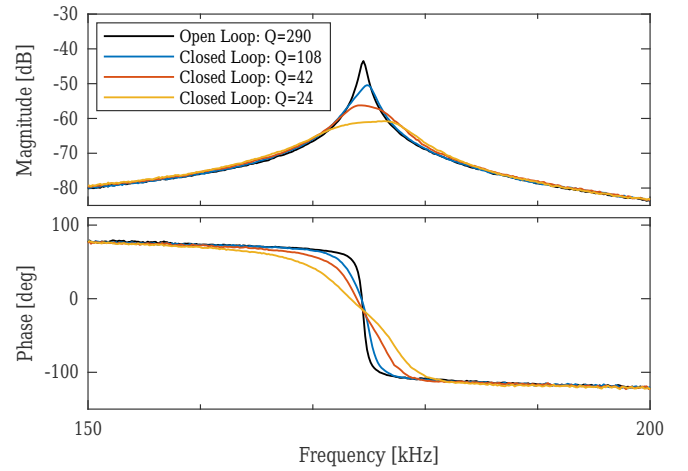


Fig. 10. Experimental frequency responses of the open-loop photothermally driven cantilever in closed-loop for various Q factors.

where the cost function is the H_∞ -norm of the closed-loop system

$$\|G_{cl}(j\omega)\|_\infty = \max_\omega |G_{cl}(j\omega)|, \quad (12)$$

which corresponds to the peak gain of the frequency response (the resonance peak). The simulation results with the model and the FRD data is shown in Fig. 8. The resulting Q factor of the closed-loop FRD model is $Q^* = 4.8$. Note, that in order to achieve the lowest H_∞ -norm, this controller slightly shifts the imaginary part of the eigenvalues as well (see Fig. 8(b)) which leads to a shifted resonance frequency.

IV. EXPERIMENTAL RESULTS

The photothermal Q controller of the form (10) was implemented on a field programmable analog array (FPAA, Anadigm AN231E04) using a single biquadratic filter with transfer function

$$C_{FPAA}(s) = G_H \frac{s^2 + \frac{2\pi f_z}{Q_z} s + (2\pi f_z)^2}{s^2 + \frac{2\pi f_p}{Q_p} s + (2\pi f_p)^2}. \quad (13)$$

calculated from (10). The experimental layout is shown in Fig. 9. The measured open-loop frequency response and the measured closed-loop frequency responses are shown in Fig. 10 for a NSC14 Cr Au 160 cantilever with slightly

higher resonance frequency. The controller design routine is based on the actual measured open-loop frequency response. It can be seen that the Q factor is reduced by over an order of magnitude from 290 to 24, resulting in approximately 17.4 dB of damping. The difference to the achieved simulated damping can be attributed to additional phase drop from the interface electronics and limitations in the FPAA controller parametrization (each controller parameter in (13) has a limited range of admissible values). These limitations will be taken into account for future controller design routines.

V. CONCLUSION

A first order low-pass filter model for the photothermal excitation in series with a second order resonant cantilever model is used for model-based Q controller design. The general controller design methods including observer based state feedback, direct polynomial pole placement, and H_∞ norm minimization are discussed and simulations are shown demonstrating significant damping. The resulting second order controller is implemented on a single FPAA and experimentally demonstrated to yield an order of magnitude reduction in the Q factor. Future work will include a more accurate modeling of the thermal low-pass behavior and a robustness analysis of the Q control loop.

REFERENCES

- [1] G. Binnig, C. F. Quate, and C. Gerber, "Atomic force microscope," *Phys. Rev. Lett.*, vol. 56, pp. 930–933, March 1986.
- [2] P. Parot, Y. F. Duf re, P. Hinterdorfer, C. Le Grimellec, D. Navajas, J.-L. Pellequer, and S. Scheuring, "Past, present and future of atomic force microscopy in life sciences and medicine," *J. Mol. Recognit.*, vol. 20, no. 6, pp. 418–431, 2007.
- [3] F. J. Giessibl, "AFM's path to atomic resolution," *Materials Today*, vol. 8, no. 5, pp. 32–41, 2005.
- [4] B. Bhushan, *Springer Handbook of Nanotechnology*. Springer-Verlag Berlin Heidelberg, 2010.
- [5] Y. Martin, C. Williams, and H. Wickramasinghe, "Atomic force microscope-force mapping and profiling on a sub 100-Å scale," *J. Appl. Phys.*, vol. 61, no. 10, pp. 4723–4729, 1987.
- [6] T. Ando, N. Kodera, E. Takai, D. Maruyama, K. Saito, and A. Toda, "A high-speed atomic force microscope for studying biological macromolecules," *Proceedings of the National Academy of Sciences*, vol. 98, no. 22, pp. 12 468–12 472, 2001.
- [7] N. Kodera, D. Yamamoto, R. Ishikawa, and T. Ando, "Video imaging of walking myosin v by high-speed atomic force microscopy," *Nature*, vol. 468, no. 7320, pp. 72–76, 2010.
- [8] M. Shibata, H. Yamashita, T. Uchihashi, H. Kandori, and T. Ando, "High-speed atomic force microscopy shows dynamic molecular processes in photoactivated bacteriorhodopsin," *Nature nanotechnology*, vol. 5, no. 3, p. 208, 2010.
- [9] J. Preiner, N. Kodera, J. Tang, A. Ebner, M. Brameshuber, D. Blaas, N. Gelbmann, H. J. Gruber, T. Ando, and P. Hinterdorfer, "Iggs are made for walking on bacterial and viral surfaces," *Nature communications*, vol. 5, p. 4394, 2014.
- [10] A. P. Nievergelt, N. Banterle, S. H. Andany, P. G nczy, and G. E. Fantner, "High-speed photothermal off-resonance atomic force microscopy reveals assembly routes of centriolar scaffold protein sas-6," *Nature nanotechnology*, vol. 13, pp. 696–701, 2018.
- [11] A. Rosa-Zeiser, E. Weilandt, S. Hild, and O. Marti, "The simultaneous measurement of elastic, electrostatic and adhesive properties by scanning force microscopy: pulsed-force mode operation," *Measurement Science and Technology*, vol. 8, no. 11, pp. 1333–1338, nov 1997.
- [12] M. Pfreundschuh, D. Alsteens, M. Hilbert, M. O. Steinmetz, and D. J. M ller, "Localizing chemical groups while imaging single native proteins by high-resolution atomic force microscopy," *Nano letters*, vol. 14, no. 5, pp. 2957–2964, 2014.
- [13] M. Hilbert, A. Noga, D. Frey, V. Hamel, P. Guichard, S. H. Kraatz, M. Pfreundschuh, S. Hosner, I. Fl ckiger, R. Jaussi *et al.*, "Sas-6 engineering reveals interdependence between cartwheel and microtubules in determining centriole architecture," *Nature cell biology*, vol. 18, no. 4, p. 393, 2016.
- [14] A. P. Nievergelt, B. W. Erickson, N. Hosseini, J. D. Adams, and G. E. Fantner, "Studying biological membranes with extended range high-speed atomic force microscopy," *Scientific reports*, vol. 5, p. 11987, 2015.
- [15] G. C. Ratcliff, D. A. Erie, and R. Superfine, "Photothermal modulation for oscillating mode atomic force microscopy in solution," *Appl. Phys. Lett.*, vol. 72, no. 15, pp. 1911–1913, 1998.
- [16] J. Mertz, O. Marti, and J. Mlynek, "Regulation of a microcantilever response by force feedback," *Appl. Phys. Lett.*, vol. 62, no. 19, pp. 2344–2346, 1993.
- [17] T. Sulchek, R. Hsieh, J. D. Adams, G. G. Yaralioglu, S. C. Minne, and C. F. Quate, "High-speed tapping mode imaging with active Q control for atomic force microscopy," *Appl. Phys. Lett.*, vol. 76(11), pp. 1473–1475, 2000.
- [18] T. Sulchek, G. G. Yaralioglu, C. F. Quate, and S. C. Minne, "Characterization and optimization of scan speed for tapping-mode atomic force microscopy," *Rev. Sci. Instrum.*, vol. 73, no. 8, pp. 2928–2936, 2002.
- [19] M. G. Ruppert and S. O. R. Moheimani, "Multimode Q control in tapping-mode AFM: Enabling imaging on higher flexural eigenmodes," *IEEE Trans. Contr. Syst. Technol.*, vol. 24, no. 4, pp. 1149–1159, July 2016.
- [20] H. H lscher and U. D. Schwarz, "Theory of amplitude modulation atomic force microscopy with and without Q-control," *International Journal of Non-Linear Mechanics*, vol. 42, no. 4, pp. 608–625, 2007.
- [21] T. R. Rodriguez and R. Garcia, "Theory of Q control in atomic force microscopy," *Appl. Phys. Lett.*, vol. 82, no. 26, pp. 4821–4823, 2003.
- [22] M. Balas, "Feedback control of flexible systems," *IEEE Transactions on Automatic Control*, vol. 23, no. 4, pp. 673–679, 1978.
- [23] R. W. Stark, "Time delay Q-control of the microcantilever in dynamic atomic force microscopy," in *5th IEEE Conference on Nanotechnology, 2005.*, July 2005, pp. 259–262 vol. 1.
- [24] M. W. Fairbairn and S. O. R. Moheimani, "Resonant control of an atomic force microscope micro-cantilever for active Q control," *Rev. Sci. Instrum.*, vol. 83, no. 8, pp. 083 708–083 708–9, 2012.
- [25] M. G. Ruppert and S. O. R. Moheimani, "Multi-mode Q control in multifrequency atomic force microscopy," in *Proc. ASME Int. Design Eng. Tech. Conf. Comput. Inf. Eng. Conf. IDETC/CIE*, vol. 4. Boston, Massachusetts, USA: ASME, August 02–05 2015, p. V004T09A009.
- [26] T. Itoh and T. Suga, "Development of a force sensor for atomic force microscopy using piezoelectric thin films," *Nanotechnology*, vol. 4, no. 4, p. 218, 1993.
- [27] M. G. Ruppert and S. O. R. Moheimani, "A novel self-sensing technique for tapping-mode atomic force microscopy," *Rev. Sci. Instrum.*, vol. 84, no. 12, p. 125006, 2013.
- [28] M. G. Ruppert and S. O. R. Moheimani, "High-bandwidth multimode self-sensing in bimodal atomic force microscopy," *Beilstein Journal of Nanotechnology*, vol. 7, pp. 284–295, 2016.
- [29] M. G. Ruppert, S. I. Moore, M. Zawiarta, A. J. Fleming, G. Putrino, and Y. K. Yong, "Multimodal atomic force microscopy with optimized higher eigenmode sensitivity using on-chip piezoelectric actuation and sensing," *Nanotechnology*, vol. 30, no. 8, p. 085503, 2019.
- [30] M. G. Ruppert and Y. K. Yong, "Note: Guaranteed collocated multimode control of an atomic force microscope cantilever using on-chip piezoelectric actuation and sensing," *Rev. Sci. Instrum.*, vol. 88, no. 8, p. 086109, Aug. 2017.
- [31] I. Petersen and A. Lanzon, "Feedback control of negative-imaginary systems," *IEEE Control Systems Magazine*, vol. 30, no. 5, pp. 54–72, 2010.
- [32] D. Ramos, J. Tamayo, J. Mertens, and M. Calleja, "Photothermal excitation of microcantilevers in liquids," *Journal of Applied Physics*, vol. 99, no. 12, p. 124904, 2006.
- [33] G. C. Goodwin, S. F. Graebe, and M. E. Salgado, *Control System Design*. Prentice Hall New Jersey, 2001, vol. 240.
- [34] K. Ogata, *Modern Control Engineering*. Prentice Hall, 2010, vol. 5.